frontiers | Frontiers in Earth Science

ORIGINAL RESEARCH
published: 26 April 2022
doi: 10.3389/feart.2022.833609

Shale Heavy Metal Isotope Records of Low Environmental O_2 Between Two Archean Oxidation Events

Chadlin M. Ostrander[1,2], Brian Kendall[3], Gwyneth W. Gordon[4,5], Sune G. Nielsen[2,6], Wang Zheng[7] and Ariel D. Anbar[4,8]*

[1]Department of Marine Chemistry and Geochemistry, Woods Hole Oceanographic Institution, Woods Hole, MA, United States, [2]NIRVANA Laboratories, Woods Hole Oceanographic Institution, Woods Hole, MA, United States, [3]Department of Earth and Environmental Sciences, University of Waterloo, Waterloo, ON, Canada, [4]School of Earth and Space Exploration, Arizona State University, Tempe, AZ, United States, [5]Knowledge Enterprise, Arizona State University, Tempe, AZ, United States, [6]Department of Geology and Geophysics, Woods Hole Oceanographic Institution, Woods Hole, MA, United States, [7]Institute of Surface-Earth System Science, School of Earth System Science, Tianjin University, Tianjin, China, [8]School of Molecular Sciences, Arizona State University, Tempe, AZ, United States

Evidence of molecular oxygen (O_2) accumulation at Earth's surface during the Archean (4.0–2.5 billion years ago, or Ga) seems to increase in its abundance and compelling nature toward the end of the eon, during the runup to the Great Oxidation Event. Yet, many details of this late-Archean O_2 story remain under-constrained, such as the extent, tempo, and location of O_2 accumulation. Here, we present a detailed Fe, Tl, and U isotope study of shales from a continuous sedimentary sequence deposited between ~2.6 and ~2.5 Ga and recovered from the Pilbara Craton of Western Australia (the Wittenoom and Mt. Sylvia formations preserved in drill core ABDP9). We find a progressive decrease in bulk-shale Fe isotope compositions moving up core (as low as $\delta^{56}Fe = -0.78 \pm 0.08‰$; 2SD) accompanied by invariant authigenic Tl isotope compositions (average $\varepsilon^{205}Tl_A = -2.0 \pm 0.6$; 2SD) and bulk-shale U isotope compositions (average $\delta^{238}U = -0.30 \pm 0.05‰$; 2SD) that are both not appreciably different from crustal rocks or bulk silicate Earth. While there are multiple possible interpretations of the decreasing $\delta^{56}Fe$ values, many, to include the most compelling, invoke strictly anaerobic processes. The invariant and near-crustal $\varepsilon^{205}Tl_A$ and $\delta^{238}U$ values point even more strongly to this interpretation, requiring reducing to only mildly oxidizing conditions over ten-million-year timescales in the late-Archean. For the atmosphere, our results permit either homogenous and low O_2 partial pressures (between $10^{-6.3}$ and 10^{-6} present atmospheric level) or heterogeneous and spatially restricted O_2 accumulation nearest the sites of O_2 production. For the ocean, our results permit minimal penetration of O_2 in marine sediments over large areas of the seafloor, at most sufficient for the burial of Fe oxide minerals but insufficient for the burial of Mn oxide minerals. The persistently low background O_2 levels implied by our dataset between ~2.6 and ~2.5 Ga contrast with the timeframes immediately before and after, where strong evidence is presented for transient Archean Oxidation Events. Viewed in this broader context, our data support the emerging narrative that Earth's initial oxygenation was a dynamic process that unfolded in fits-and-starts over many hundreds-of-millions of years.

Keywords: archean, thallium, iron, uranium, isotopes, oxygen

OPEN ACCESS

Edited by:
Julia Ribeiro, Guangzhou Institute of Geochemistry (CAS), China

Reviewed by:
Ross Raymond Large, University of Tasmania, Australia
Martin Wille, University of Bern, Switzerland

****Correspondence:***
Chadlin M. Ostrander
costrander@whoi.edu

Specialty section:
This article was submitted to Geochemistry, a section of the journal Frontiers in Earth Science

Received: *11 December 2021*
Accepted: *16 March 2022*
Published: *26 April 2022*

Citation:
Ostrander CM, Kendall B, Gordon GW, Nielsen SG, Zheng W and Anbar AD (2022) Shale Heavy Metal Isotope Records of Low Environmental O_2 Between Two Archean Oxidation Events. Front. Earth Sci. 10:833609. doi: 10.3389/feart.2022.833609

INTRODUCTION

Earth's earliest O_2 history remains a topic of ongoing debate (compare Kopp et al., 2005 against Ohmoto et al., 2006 for two extreme end-member scenarios), and many important details remain unresolved. For example, evidence of O_2 production and accumulation increases in both its abundance and compelling nature in the immediate runup to the Great Oxidation Event (GOE), during the final few hundred million years of the Archean Eon (4.0–2.5 Ga; summarized in Ostrander et al., 2021). Two Archean Oxidation Events (AOEs), each of probably single-million-years duration, have been identified during the late-Archean and verified by multiple lines of independent evidence: one at ~2.65 Ga (Koehler et al., 2018; Olson et al., 2019; Ostrander et al., 2020) and another at ~2.50 Ga (Anbar et al., 2007; Kaufman et al., 2007; Wille et al., 2007; Garvin et al., 2009; Godfrey and Falkowski 2009; Reinhard et al., 2009; Duan et al., 2010; Kendall et al., 2010, 2013, 2015a; Gregory et al., 2015; Kurzweil et al., 2015; Stüeken et al., 2015; Ostrander et al., 2019, 2020; Meixnerová et al., 2021). Evidence is also presented for non-zero and fluctuating O_2 levels during the much longer intervening timeframe (e.g., Eigenbrode and Freeman 2006, Stüeken et al., 2012, Gregory et al., 2015, Eroglu et al., 2015; 2017); however, this evidence is at times not as compelling, and follow-up studies of the same and coeval samples oftentimes arrive at different conclusions. For example, progressively heavier Mo isotope compositions are found in sedimentary rocks formed between about 2.6 and 2.5 Ga and inferred as evidence of a progressive rise in atmospheric and oceanic O_2 levels (Wille et al., 2007; Kurzweil et al., 2015). Yet, in some of these same rocks, generally invariant C (Fischer et al., 2009) and U (Brüske et al., 2020) isotope compositions are inferred as evidence of little to no change to Earth's surface O_2 levels. To summarize, emerging evidence clearly identifies brief, single-million-year O_2 accumulation events on the eve of the GOE, but no clear consensus yet exists for the O_2 levels that persisted over much longer, tens-of-million-year timeframes.

What is missing up to this point, and provided here, is a detailed, multi-pronged geochemical investigation of a continuous sedimentary sequence deposited during the late-Archean. We generated Fe, Tl, and U isotope records from shales of the Wittenoom and Mt. Sylvia formations (Western Australia) deposited between about 2.6 and 2.5 Ga and recovered from the ABDP9 drill core. Each of these heavy metal isotope "paleoredox proxies" is uniquely sensitive to a specific redox threshold; Fe isotopes are directly sensitive to Fe oxidation (Johnson et al., 2008), U isotopes are directly sensitive to U oxidation (Tissot and Dauphas 2015), and Tl isotopes are indirectly sensitive to Mn oxidation (Nielsen et al., 2017). Each of these proxies is also already proven independently valuable in reconstructing atmospheric and oceanic O_2 levels during the Archean (e.g., Fe: Rouxel et al., 2005, Czaja et al., 2012, Heard et al., 2020, U: Kendall et al., 2013, Wang et al., 2018; 2020, Brüske et al., 2020, and Tl: Ostrander et al., 2019). Our study represents the first time ever, at any time in Earth's past, all three proxies are applied in a single study to the same sedimentary archive.

HEAVY METAL ISOTOPE PROXIES

Fe Isotope Proxy

Sedimentary Fe isotope ratios have the potential to trace ancient Fe redox reactions. A large equilibrium isotope fractionation effect is imparted during Fe redox reactions that can leave the Fe(II) phase up to ~3.0‰ lighter than the Fe(III) phase (Welch et al., 2003). Sediments today and their constituent minerals are shown to capture and preserve these Fe isotopic effects, at least partially (e.g., Severmann et al., 2008; Busigny et al., 2014; Scholz et al., 2014). Likewise, and by analogy, fingerprints of Fe redox reactions in Archean oceans should be left behind in the Archean sedimentary record. Indeed, a large degree of Fe isotope variability is found in Archean sedimentary rocks and interpreted as evidence of ancient Fe redox reactions (e.g., Rouxel et al., 2005; Czaja et al., 2012; Heard et al., 2020).

There are some caveats to the Fe isotope proxy. Iron redox reactions cannot be explicitly linked to aerobic processes; oxidation of Fe(II) is observed in the absence of O_2 during interaction with UV-light (Cairns-Smith 1978) and also during photo-ferrotrophy (Widdel et al., 1993). Furthermore, there exist at least two means for driving considerable Fe isotope fractionation effects without the requirement of an Fe redox change: hydrothermal processes (by up to ~0.7‰; Lough et al., 2017) and pyrite formation (by up to ~3.0‰; Guilbaud et al., 2011). These caveats can make it extremely difficult, and at times even impossible to differentiate anaerobic from aerobic redox processes using Fe isotopes alone. Notwithstanding, useful information can still be gleaned from the proxy in deep time when it is applied in tandem with other, complementary proxies (e.g., Czaja et al., 2012; Asael et al., 2013).

U Isotope Proxy

When applied to the Archean sedimentary record, the U isotope paleoredox proxy has emerged as a useful tracer of early U(IV) oxidation. On the modern well-oxygenated Earth, U(IV) is readily oxidized to U(VI) during oxidative weathering and delivered to the ocean as the soluble uranyl carbonate complex [$UO_2(CO_3)_3^{4-}$; Langmuir 1978], where it accumulates with a residence time (~400 kyr; Ku et al., 1977) that far exceeds the ocean mixing time (~1 kyr; Sarmiento and Gruber 2006). Within the U(VI)-replete modern marine realm, U is readily exchanged between seawater and sediments, and this leads to a large range of U isotope ratios across different sediment types ($\Delta^{238}U$ = ~1.3‰; Weyer et al., 2008; Tissot and Dauphas 2015). By contrast, on a primarily anoxic Archean Earth, it would be expected that U(IV) oxidation would be negligible or non-existent, at the very least stunting and in the most extreme case preventing U(VI) accumulation in seawater. In an ocean devoid of mobile U(VI), there would be no opportunity for

isotopic fractionation between seawater and marine sediments.

Following from this logic, U isotopes have been treated essentially as a binary paleoredox proxy when applied to the Archean Eon. When free-O_2 was in low abundance or non-existent, sedimentary rocks should reveal minimal U enrichments and $\delta^{238}U$ values indistinguishable from, or very close to, average upper continental crust and the mantle (both possess $\delta^{238}U$ = −0.3‰; Partin et al., 2013; Brüske et al., 2020; Chen et al., 2021). In contrast, during episodes of appreciable O_2 accumulation, sedimentary rocks should reveal some combination of U enrichments and non-crustal $\delta^{238}U$ values (Kendall et al., 2013; Wang et al., 2018).

Tl Isotope Proxy

The Tl isotope paleoredox proxy is the youngest of the three isotope systems, having emerged relatively recently as a novel tool for tracking changes in ancient marine oxygenation indirectly through Mn oxide burial (Nielsen et al., 2011; Owens et al., 2017). The strongest isotopic lever of seawater Tl isotope mass-balance today is Mn oxide minerals that get buried in well-oxygenated marine sediments (Baker et al., 2009). Manganese oxides possess a strong preference for the heavier-mass Tl isotope ($\varepsilon^{205}Tl$ = +10 to +14; Rehkämper et al., 2002; Nielsen et al., 2013), and their widespread distribution on the well-oxygenated seafloor today leads to accumulation of the lighter-mass Tl isotope in seawater ($\varepsilon^{205}Tl$ = −6.0 ± 0.3; Nielsen et al., 2006a; Owens et al., 2017) relative to global oceanic Tl inputs ($\varepsilon^{205}Tl$ = −1.8; Nielsen et al., 2017). Because the residence time of Tl in seawater today (~19 kyr; Nielsen et al., 2017) exceeds the ocean mixing time, the seawater $\varepsilon^{205}Tl$ signature today is globally homogenous. By contrast, Fe oxide minerals are unlikely to fractionate Tl isotopes because the likely fractionation mechanism—oxidation of Tl(I) to Tl(III)—does not occur during sorption to Fe oxides (Peacock and Moon 2012). Moreover, neither of the two remaining primary marine Tl outputs today imparts a substantial isotopic fractionation effect; low-temperature oceanic crust alteration imparts only a slight negative isotope fractionation effect (average $\varepsilon^{205}Tl$ = −7.2; Nielsen et al., 2017), and no isotope fractionation is observed in Tl leached from pyrite from sediments deposited under anoxic bottom waters, presumably because of quantitative Tl transfer to pyrite in these settings (Owens et al., 2017; Fan et al., 2020; Chen et al., 2022).

Akin to U isotopes, Tl isotopes can also be treated as a binary proxy when applied to the Archean. In the absence of the Mn oxide mass-balance lever—for example, in a widely anoxic Archean ocean—the seawater $\varepsilon^{205}Tl$ value will not be significantly different from that of the bulk upper continental crust and mantle (roughly $\varepsilon^{205}Tl$ = −2.0 ± 1.0; Nielsen et al., 2005; 2006b). By analogy with modern equivalents, pyrite leached from Archean sedimentary rocks deposited under anoxic conditions should capture this near-crustal seawater $\varepsilon^{205}Tl$ value (Owens et al., 2017). In support of this logic, near-crustal $\varepsilon^{205}Tl_A$ values are found in pyrite leached from shales deposited under locally anoxic conditions at a time of inferred low Archean O_2 levels, with a deviation toward more negative $\varepsilon^{205}Tl_A$ values found exclusively during a transient 2.5 Ga AOE (compare $\varepsilon^{205}Tl_A$ between the lower and upper Mt. McRae Shale in ABDP9; Ostrander et al., 2019).

MATERIALS AND METHODS

Drill Core ABDP9

Drill core ABDP9 was recovered from the Pilbara Craton of Western Australia during the 2004 NASA Astrobiology Institute Deep Time Drilling Project (**Figure 1**). Detailed descriptions of the core are provided in previous work (Anbar et al., 2007; Kaufman et al., 2007); we offer only a brief summary here. Shales are the dominant lithology in the lowermost and middle Wittenoom Formation, with organic-rich ("black") shales becoming increasingly common in the uppermost Wittenoom and overlying Mt. Sylvia Formation. Intervals of banded iron formation (BIF) deposition are present but infrequent, appearing in the middle of the Wittenoom Formation and near the base and top of the Mt. Sylvia Formation. Intervals of BIF deposition were avoided, and care was also taken to avoid depths containing macroscopic pyrite. Sedimentary rocks in ABDP9 have experienced relatively minor metamorphism considering their age (prehnite-pumpellyite facies, < 300°C; Brocks et al., 2003).

According to available geochronological constraints, the Wittenoom and Mt. Sylvia formations were deposited between about 2.6 and 2.5 Ga (Trendall et al., 2004). Wittenoom Formation deposition initiated sometime after 2.597 ± 0.005 Ga according to a zircon U–Pb age for volcanoclastics from the underlying Marra Mamba Formation (Trendall et al., 1998). A Pb-Pb age of 2.541 ± 0.018 Ga was obtained for an impact spherule bed found in coeval carbonaceous strata at a nearby location (Woodhead et al., 1998), and it is suggested that a contemporaneous spherule bed is present in ABDP9 at 295 m core depth (Kurzweil et al., 2015). An upper age limit of 2.495 ± 0.014 Ga for the Mt. Sylvia Formation comes from a Re–Os depositional age for organic-rich shales from the overlying Mt. McRae Shale in ABDP9 (Kendall et al., 2015a).

Deposition of shales from ABDP9 is thought to have taken place below storm wave base on the outer-shelf in a marginal or open-ocean setting (Morris and Horwitz 1983). According to previously published Fe speciation, trace metal, and Mo isotope data, shales from the Wittenoom and Mt. Sylvia formations were deposited under the anoxic conditions that typified most Archean marine environments (Ostrander et al., 2020). Localized anoxia seems to have persisted throughout deposition of both units, and there is a possibility that redox conditions were especially reducing during deposition of the Mt. Sylvia Formation. In the uppermost Wittenoom Formation, above around 250 m core depth, there is an increase in the ratio of total Fe (Fe_T) to Al and in the ratio of highly reactive Fe (Fe_{HR}) to Fe_T (**Figure 2**). Although there is no comparable trend in the ratio of pyritized Fe (Fe_{Py}) to Fe_{HR}, ratios indicative of euxinic conditions are approached for the first time in the section at around this same depth. By analogy with modern analogs, each of these changes in Fe

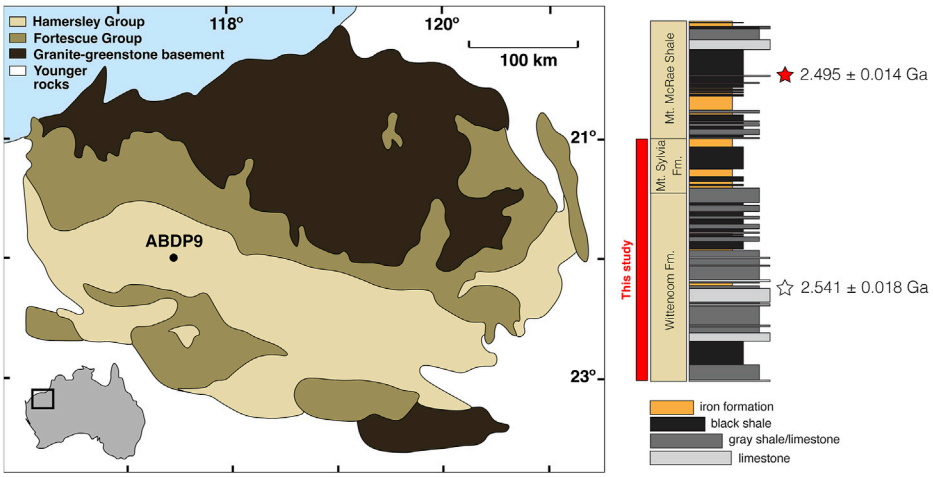

FIGURE 1 | Geological map of the Pilbara Craton and ABDP9 stratigraphy. Geological map is modified from Kurzweil et al. (2015) and stratigraphy is modified from Anbar et al. (2007) and Ostrander et al. (2020). Age constraints are from, in ascending order, Woodhead et al. (1998) and Kendall et al. (2015a).

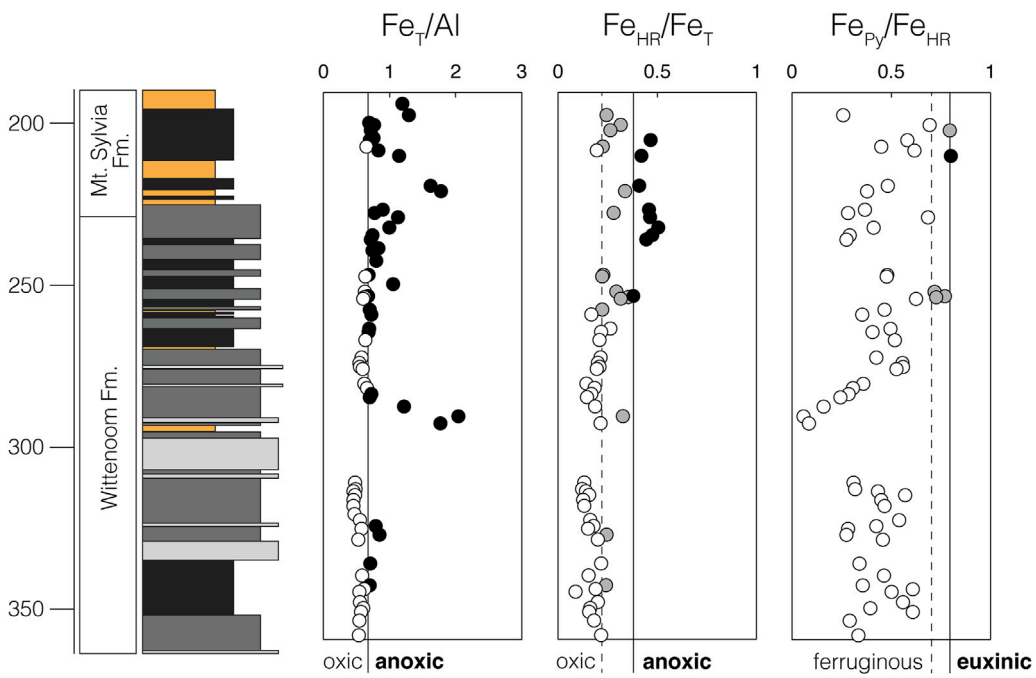

FIGURE 2 | Previously published Fe speciation data indicating persistent localized anoxia during deposition of the Wittenoom and Mt. Sylvia formations in ABDP9. Data and original interpretation are from Ostrander et al. (2020). Black datapoints exceed strict thresholds for local anoxia ($Fe_T/Al > 0.55$ or $Fe_{HR}/Fe_T > 0.38$) or euxinia ($Fe_{Py}/Fe_{HR} > 0.80$), while gray datapoints exceed relaxed thresholds for the same ($Fe_{HR}/Fe_T > 0.22$ for anoxia and $Fe_{Py}/Fe_{HR} > 0.70$ for euxinia) (summarized in Raiswell et al., 2018).

speciation would be an expected consequence of strengthened local anoxia (Raiswell et al., 2018). Previously published Mo isotopic compositions from Ostrander et al. (2020) are also heavier in the Mt. Sylvia Formation (δ^{98}Mo up to 1.43‰, and averaging 0.97‰) than in the Wittenoom Formation (δ^{98}Mo up to 1.02‰, and averaging 0.73‰) in ABDP9, which could also support more reducing local redox conditions during deposition of the former by analogy with modern equivalents (Kendall et al., 2017; but see Kurzweil et al., 2015 for an alternative interpretation that attributes these increasing δ^{98}Mo values to progressive Earth surface oxidation).

The Wittenoom and Mt. Sylvia formations were deposited in a timeframe separating two transient AOEs. Redox-sensitive trace metal enrichments are found in the ~2.65 Ga Jeerinah Formation and interpreted as evidence of oxidative sulfide weathering on land [Se up to 5 ug/g (Koehler et al., 2018) and Mo up to 10 ug/g (Olson et al., 2019)]. Heavy N isotope compositions in the same samples support coeval marine oxygenation by fingerprinting the operation of an aerobic N cycle in overlying waters (up to $\delta^{15}N$ = ~6.0‰; Koehler et al., 2018), an interpretation that gains support from heavy Se and Mo isotope compositions that imply removal of lighter-mass isotopes in shallower-water, mildly oxygenated sediments on the continental shelf (up to $\delta^{82}Se$ = 0.90‰ (Koehler et al., 2018) and up to $\delta^{98}Mo$ = 1.01‰ (Ostrander et al., 2020)). These geochemical patterns are even more pronounced in the upper member of the Mt. McRae Shale in ABDP9, indicating that an especially pronounced AOE took place at ~2.50 Ga. During this younger AOE, oxidative weathering is indicated by strong trace metals enrichments (Se up to 20 ug/g (Stüeken et al., 2015) and Mo up to 49 ug/g (Anbar et al., 2007)). Heavy N isotope values again support a local aerobic N cycle (up to $\delta^{15}N$ = 7.5‰; Garvin et al., 2009), and even heavier Se and Mo isotope compositions imply more pronounced removal of lighter-mass isotopes in mildly oxygenated settings on the continental shelf (up to $\delta^{82}Se$ = 1.43‰ (Stüeken et al., 2015) and up to $\delta^{98}Mo$ = 1.77‰ (Duan et al., 2010)). Other geochemical trends found in the upper Mt. McRae Shale also corroborate the AOE hypothesis, as do those found in coeval shales from South Africa (summarized in Ostrander et al., 2021).

Isotopic Methods

For Fe and U, sample preparation, isotope purification, and analyses were conducted at the Metals, Environment, Terrestrial Analytical Laboratory (METAL) at Arizona State University. About one-hundred milligrams of whole-rock material from each sample depth was powdered and ashed overnight in a muffle furnace at 550°C to oxidize organic material. Then, each sample was transferred to a trace metal clean lab where it was subjected to multiple rounds of concentrated acid digestion using trace metal grade hydrofluoric, hydrochloric, and nitric acids in pre-cleaned Teflon labware. Once completely dissolved, samples were transferred to trace-metal clean screw top bottles ("stock solution"), from which a small aliquot was taken and diluted in 2% nitric acid in preparation for concentration analysis on a Thermo Scientific X-series quadrupole ICP-MS following published methods (Anbar et al., 2007; Kendall et al., 2010). Isotope purification and analysis was conducted following procedures outlined in previous Fe (Beard et al., 2003; Arnold et al., 2004) and U (Weyer et al., 2008; Kendall et al., 2013) isotopic investigations. A stock solution split equivalent to 10 µg of Fe was separated from the sample matrix via ion exchange chromatography using Bio-Rad AG1X8 anion resin. To avoid isotopic fractionation associated with ion exchange purification, only samples recovering ≥95% of their original Fe contents were prepared for isotopic analysis (this was checked *via* ICP-MS). Samples that fit this criterion were dried down, brought up in 0.32 M HNO_3, and doped with a NIST 3114 Cu elemental spike to correct for instrumental mass bias during isotopic analysis. Thereafter, a separate split equivalent to 250 ng of U was taken from each stock solution and mixed with a $^{236}U/^{233}U$ double-spike solution to correct for instrumental mass bias during purification and isotopic analysis. Samples were purified using Eichrom® UTEVA resin, dried-down, and reconstituted in 0.32 M HNO_3 in preparation for isotopic analysis. Fe and U isotope ratio measurements were performed on a Thermo Neptune multi-collector ICPMS (MC-ICP-MS) in medium- and low-resolution mode, respectively, utilizing sample-standard bracketing. For Fe, IRMM-524a was used as the bracketing standard, which is shown to be isotopically indistinguishable from IRMM-014 (Craddock and Dauphas, 2011). All bulk-shale Fe isotope data are reported relative to IRMM-524a in delta notation:

$$\delta^{56}\mathrm{Fe}\ (‰) = \left(^{56/54}\mathrm{Fe}_{\mathrm{sample}} \div {}^{56/54}\mathrm{Fe}_{\mathrm{IRMM-524a}} - 1\right) \times 1{,}000.$$

For U, CRM 145 was used as the bracketing standard and all bulk-shale data are reported relative to this standard in delta notation:

$$\delta^{238}\mathrm{U}\ (‰) = \left(^{238/235}\mathrm{U}_{\mathrm{sample}} \div {}^{238/235}\mathrm{U}_{\mathrm{CRM\,145}} - 1\right) \times 1{,}000.$$

Sample preparation and analysis for Tl were conducted at the NIRVANA Laboratory at Woods Hole Oceanographic Institution (WHOI) and the WHOI Plasma Mass Spectrometry Facility. About one-hundred milligrams of powdered shale material from each sample depth was transferred to a Teflon reactor and treated with 2 M HNO_3 for 12–15 h at 130°C, a treatment shown to effectively "leach" authigenic Tl bound to pyrite from detrital Tl (Nielsen et al., 2011). Following this partial dissolution, samples were centrifuged, and their supernatants containing the authigenic fraction were transferred to new Teflon reactors and digested using trace metal grade concentrated HCl and HNO_3. Once dissolved, samples were reconstituted in 1 M HCl in preparation for Tl purification via the typical two-step ion-exchange chromatography procedure (using AG1X8 anion resin; Rehkämper and Halliday 1999; Nielsen et al., 2004). Thallium isotope ratio measurements were performed using previously established techniques (Rehkämper and Halliday 1999; Nielsen et al., 2004) on a Thermo Neptune MC-ICP-MS equipped with an Aridus II desolvating nebulizer sample introduction system in low-resolution mode. Sample-standard bracketing was conducted relative to NIST 997 Tl, and instrumental mass bias correction was done by external normalization to NIST SRM 981 Pb. Because each sample was doped with a known quantity of NIST SRM 981 Pb, authigenic Tl concentrations could be calculated during MC-ICPMS analysis using the measured $^{205}Tl/^{208}Pb$ ratios. We report all authigenic Tl isotope values in epsilon notation relative to NIST 997 Tl metal:

$$\varepsilon^{205}\mathrm{Tl}_{\mathrm{A}} = \left(^{205/203}\mathrm{Tl}_{\mathrm{sample}} \Big/ {}^{205/203}\mathrm{Tl}_{\mathrm{NIST-997}} - 1\right) \times 1{,}000.$$

USGS rock reference materials were simultaneously processed with each batch of samples and showed good reproducibility, as did various previously processed standard solutions (**Table 1**). Reported uncertainties for our samples are always in 2SD and either equal to the highest 2SD reproducibility of our standards or the individual sample's reproducibility, whichever is greater. All data are provided in the **Supplementary Material**.

TABLE 1 | Standard isotope data.

Fe isotope standards	δ^{56}Fe (2SD)	N	Previously published values (2SD)
BIR	0.07 (0.05)[a]	4	0.05 (0.02)[b]
Tag Fe	−0.86 (0.08)[a]	7	−0.99 (0.09)[c]
SDO-1	0.04 (0.07)[d]	8	−0.05 (0.12)[c]
U isotope standards	δ^{238}U (2SD)	N	Previously published values (2SD)
CRM129A	−1.72 (0.09)[a]	12	−1.71 (0.05)[e]
Ricca	−0.22 (0.11)[a]	14	−0.23 (0.06)[e]
SDO-1	−0.11 (0.09)[d]	6	−0.06 (0.04)[f]
Tl isotope standard	ε^{205}Tl (2SD)	N	Previously published values (2SD)
SCO-1	−2.9 (0.2)[d]	4	−2.6 (0.2)[g]

[a]*Previously digested and purified standard solution.*
[b]*Value reported by Craddock and Dauphas (2011).*
[c]*Value reported by Severmann et al. (2008).*
[d]*Powdered rock standard digested and purified alongside samples.*
[e]*Value reported by Zhang et al. (2018).*
[f]*value reported by Kendall et al. (2015b).*
[g]*value reported by Ostrander et al. (2017).*

RESULTS

We find a general decrease in bulk-shale δ^{56}Fe values moving up section (**Figure 3**). At and below 259.04 m, δ^{56}Fe values are generally invariant (average δ^{56}Fe = –0.01 ± 0.42‰; 2SD), with only one sample (δ^{56}Fe = +0.54 ± 0.14‰ at 292.74 m) possessing a δ^{56}Fe value vastly different from that of modern bulk upper continental crust ($\delta^{56}Fe_{BUCC} \approx 0.00$‰; Dauphas et al., 2017). At and above 253.17 m, δ^{56}Fe values become progressively lower, reaching a minimum of –0.78 ± 0.08‰ (at 228.70 m) and averaging –0.51 ± 0.36‰. Bulk-shale Fe abundances are fairly constant throughout the sedimentary sequence (averaging 5.4 wt%), with the exception of two instances of noticeable Fe enrichment near Fe-formation intervals in the middle of the Wittenoom Formation (as high as 14.2 wt% at 290.52 m) and near the base of the Mt. Sylvia Formation (as high as 10.9 wt% at 218.91 m) (**Figure 4**). These Fe enrichment trends mirror those of the Fe/Al data (**Figure 2**).

In contrast, δ^{238}U and $\varepsilon^{205}Tl_{auth}$ values are invariant and always within uncertainty of their respective modern bulk upper continental crust values. Bulk-shale δ^{238}U values average –0.30 ± 0.06‰ (2SD) in the Wittenoom Formation and –0.29 ± 0.03‰ (2SD) in the Mt. Sylvia Formation (**Figure 3**); both are identical to the estimated modern BUCC δ^{238}U value of –0.29 ± 0.03‰ (Tissot and Dauphas 2015). Authigenic ε^{205}Tl values average –1.97 ± 0.60 (2SD) in the Wittenoom Formation and –2.15 ± 0.51 (2SD) in the Mt. Sylvia Formation (**Figure 3**); both are indistinguishable from the estimated modern BUCC ε^{205}Tl value of –2.1 ± 1.3 (Nielsen et al., 2005). Bulk-shale U concentrations slightly decrease moving up section (averaging 4.3 μg/g in the Wittenoom Formation and 3.0 μg/g in the Mt. Sylvia Formation), a trend that is also preserved when normalized to Al (**Figure 4**). Authigenic Tl concentrations are slightly lower

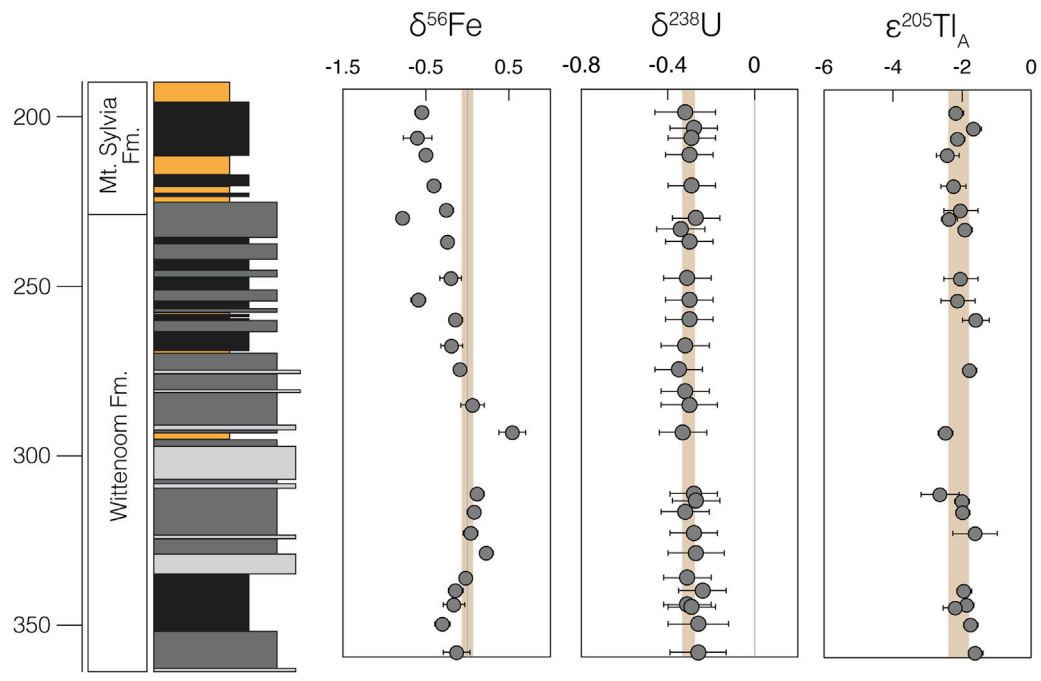

FIGURE 3 | Heavy metal isotope data generated during the current study. δ^{56}Fe and δ^{238}U values are for bulk-shale, while $\varepsilon^{205}Tl_A$ values are for leached (authigenic) fractions. The brown shaded region in each panel represents the estimated average bulk upper continental crust value for that isotope system, which is in all cases similar to the estimated mantle value. Errors are either equal to the highest 2SD reproducibility of our standards or the individual sample's reproducibility, whichever is greater.

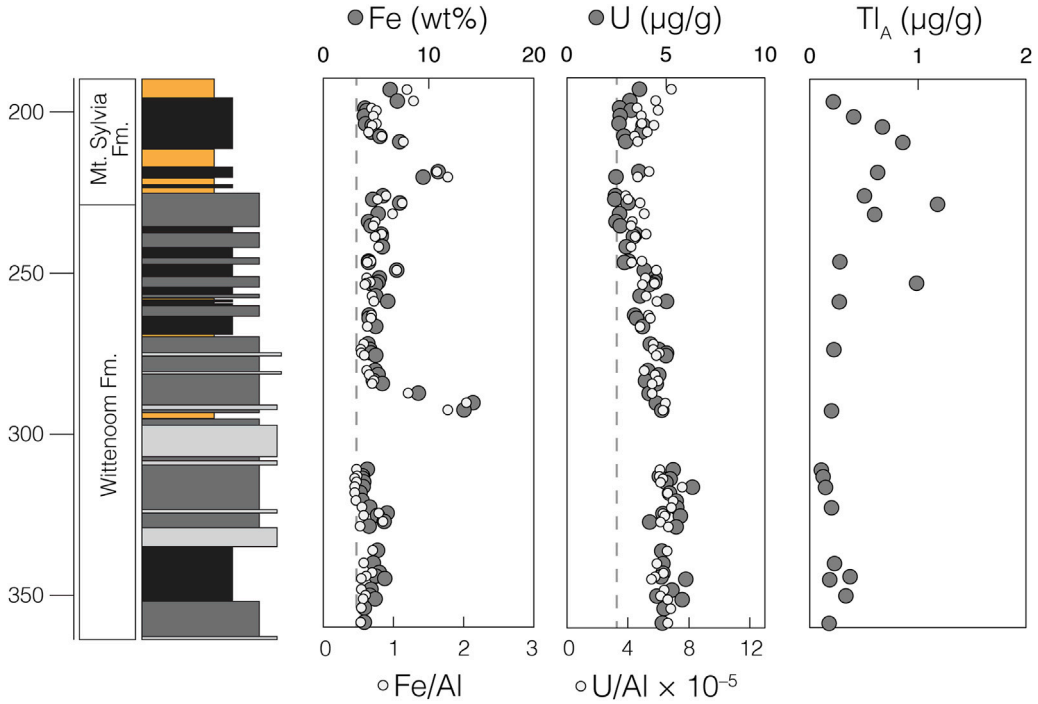

FIGURE 4 | Trace metal concentration data generated during the current study. Dark gray datapoints represent non-normalized concentrations for bulk-shale (Fe and U) and leached authigenic fractions (Tl_A). Light gray datapoints represent concentrations normalized to the non-redox sensitive element Al and gray dashed lines represent average upper continental crust values for these ratios (Rudnick and Gao 2003).

in the Wittenoom Formation (averaging 0.3 μg/g) compared to the Mt. Sylvia Formation (averaging 0.6 μg/g) (**Figure 4**).

DISCUSSION

Fe Isotope Data

As an initial step in interpreting the δ^{56}Fe data, it is important to estimate the authigenic Fe isotope contribution to each sample. The Fe in each shale sample is primarily a mixture of two components: a detrital fraction (i.e., continent-derived; f_D) and an authigenic fraction (i.e., seawater-derived; f_A). The latter is more important for tracking changes in ancient low-temperature geochemical processes. If we assume the sum of these two fractions is equal to one ($f_D + f_A = 1$), then the following equation can be used to calculate f_A:

$$f_A = 1 - (Al \times (Fe/Al)_D \div Fe).$$

where "Al" and "Fe" signify bulk shale sample concentrations, and $(Fe/Al)_D$ represents the inverted ratio of these elements in the detrital component. Because Al is not redox-sensitive, increases in shale Fe/Al ratios above the detrital background are most likely due to the preferential accumulation of authigenic Fe (e.g., Lyons and Severmann 2006). For Fe/Al_D we use 0.45, the lowest Fe/Al ratio found in our shale samples, because this value is the least likely to contain an authigenic Fe enrichment. This ratio is very similar to that estimated for the modern bulk upper continental crust (BUCC) of 0.48 (Rudnick and Gao 2003), the source of detrital material.

When calculated f_A are plotted versus their respective bulk-shale δ^{56}Fe values, a coherent relationship is revealed ($R^2 = 0.52$ when the lone sample with an especially high δ^{56}Fe value of 0.54 ± 0.16‰ is omitted; **Figure 5**). Samples with especially low f_A possess bulk-shale δ^{56}Fe values that most closely resemble modern BUCC (leftmost data in **Figure 5**). These samples are strongly affected by their high detrital Fe contributions. In contrast, samples with especially high f_A reveal continuously decreasing bulk-shale δ^{56}Fe values (rightmost data in **Figure 5**). These samples are not affected by high detrital Fe contributions, and as such are ideal for reconstructing the authigenic Fe source. Omitting one sample with an especially high bulk-shale δ^{56}Fe value, and also samples with especially high detrital Fe contributions (specifically, three samples with $f_A <$ 0.15), the remaining samples ($n = 19$) can be reconciled by two-component mixing between detrital Fe ($\delta^{56}Fe_{BUCC} \approx 0.00$‰; Dauphas et al., 2017) and an authigenic δ^{56}Fe source ($\delta^{56}Fe_A$) between −1.54‰ and −0.22‰ (**Figure 5A**).

It is possible that Fe oxide mineral formation in late-Archean marine settings led to the preferential removal of heavier-mass Fe isotopes, leaving behind an isotopically light seawater $\delta^{56}Fe_A$ component that was then transferred, at least partially, to our shale samples (e.g., Rouxel et al., 2005; Severmann et al., 2008). One hypothesis contends that partial oxidation of the seawater Fe reservoir led to a globally widespread and isotopically light seawater Fe reservoir (Rouxel et al., 2005). Another hypothesis

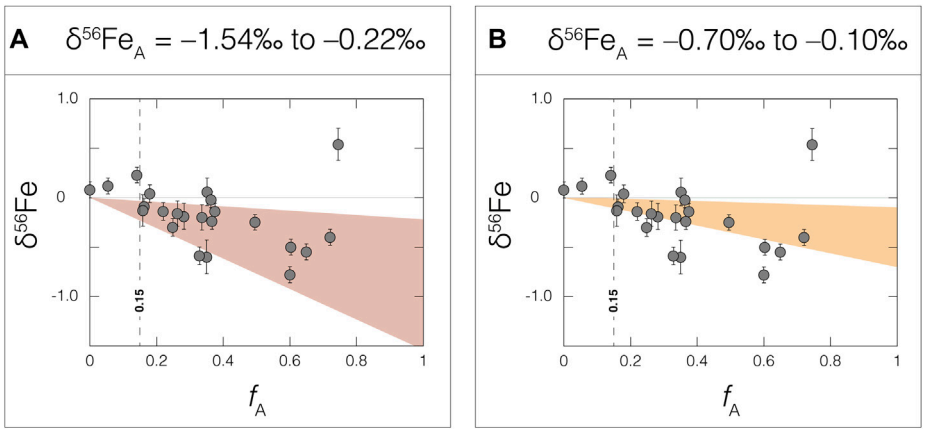

FIGURE 5 | Bulk-shale $\delta^{56}Fe$ values plotted versus calculated authigenic Fe fractions (f_A). The red field in panel **(A)** signifies an authigenic $\delta^{56}Fe$ source that can reconcile all but four datapoints ($\delta^{56}Fe$ = –1.54‰ to –0.22‰), while the orange field in panel **(B)** signifies an authigenic $\delta^{56}Fe$ source comparable to modern hydrothermal inputs ($\delta^{56}Fe_A$ = –0.70‰ to –0.10‰; Lough et al., 2017). The 0.15 vertical line in both panels represents a cut-off point, below which the Fe content present in bulk-shale samples is overwhelmingly dominated by detrital material. See the text for a description of the f_A calculation.

suggests essentially the same, just on a smaller, basinal scale (the "shuttle" hypothesis; Severmann et al., 2008). In combination with one or both Fe-oxide hypotheses, it is also suggested that local redox conditions and distance from the paleoshoreline played a strong role in how this isotopically light signal was captured in sediments, with strongly reducing and pyrite-rich euxinic conditions farther from shore being the most likely locations of capture (Ostrander et al., 2022). Interestingly, and in partial support of this idea, the appearance of lighter bulk-shale $\delta^{56}Fe$ in the Mt. Sylvia Formation coincides with the local redox transition toward more reducing conditions (see the Materials section, and also **Figure 2**). This relationship is unlikely to be coincidental. More to this point, calculated $\delta^{56}Fe_A$ values for Wittenoom Formation shales are also considerably lighter than bulk-crust (average $\delta^{56}Fe_A$ = = –0.72 ± 0.90‰; 2SD after screening out samples with positive bulk-shale $\delta^{56}Fe$ values and f_A < 0.15), indicating that an isotopically light $\delta^{56}Fe_A$ source probably persisted over longer timeframes of deposition than is evident from the bulk-shale $\delta^{56}Fe$ data alone. This light $\delta^{56}Fe_A$ source simply failed to register a strong bulk-shale $\delta^{56}Fe$ signal in some Wittenoom Formation shales because of their strong detrital Fe contents.

Alternatively, or in addition, hydrothermal Fe delivery and local pyrite formation could have helped supply an isotopically light $\delta^{56}Fe_A$ component. Of the samples with f_A > 0.15, the vast majority (74%) can be reconciled solely by a low $\delta^{56}Fe_A$ component that overlaps with modern hydrothermal fluids ($\delta^{56}Fe$ = –0.1‰ to –0.7‰; Lough et al., 2017) (**Figure 5B**). It is generally accepted that the overwhelming source of dissolved Fe(II) to Archean seawater was hydrothermal fluids (Konhauser et al., 2017). Furthermore, and again, the lowest $\delta^{56}Fe$ values are found in shales from the Mt. Sylvia Formation (**Figure 3**), perhaps coincident with a transition toward more reducing local redox conditions (see **Figure 2**). If this local redox change led to H_2S accumulation in porewaters or overlying waters, then localized pyrite formation could have led to the preferential removal of lighter-mass Fe isotopes from seawater (Guilbaud et al., 2011). The slight increase in authigenic Tl abundances observed in the Mt. Sylvia Formation (**Figure 4**) could also support enhanced local pyrite formation at this time because accumulation of Tl in sediments is often linked to pyrite (e.g., Nielsen et al., 2011). Lastly, and most convincing, shales with higher pyrite Fe contents reveal increasingly negative $\delta^{56}Fe$ values (R^2 = 0.59; **Figure 6**).

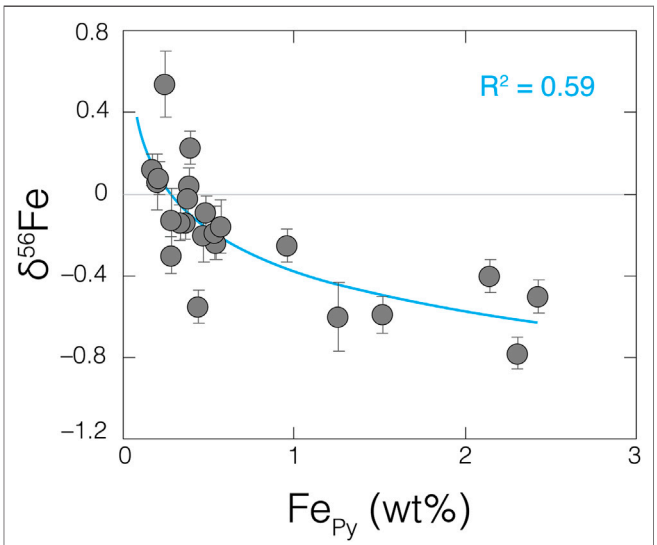

FIGURE 6 | Increasingly negative bulk-shale $\delta^{56}Fe$ values are accompanied by higher pyrite Fe contents (Fe_{Py}) in our samples, drawing a strong connection between two. Pyrite Fe data are from Ostrander et al. (2020). A logarithmic trendline through the dataset is provided in blue, along with the corresponding R^2 value.

None of the Fe isotope fractionation processes discussed above require the presence of O_2. Two anaerobic processes serve as

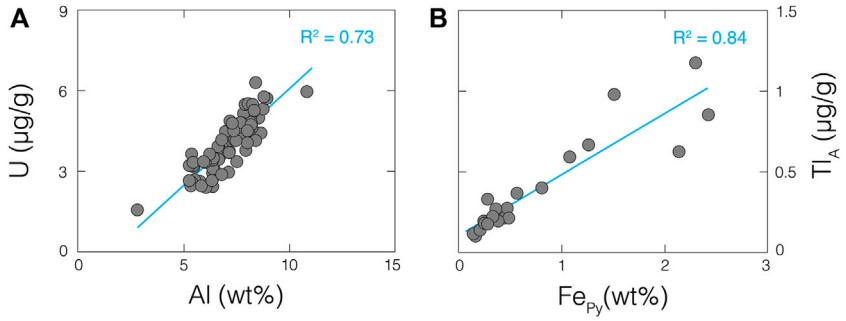

FIGURE 7 | A strong linear correlation between bulk-shale U and Al concentrations **(A)** suggests a shared detrital origin, while an even stronger linear correlation between leached Tl and pyrite Fe concentrations **(B)** suggests a strong Tl-pyrite connection. Aluminum and pyrite Fe data are from Ostrander et al. (2020). Linear trendlines are provided in blue, along with corresponding R^2 values.

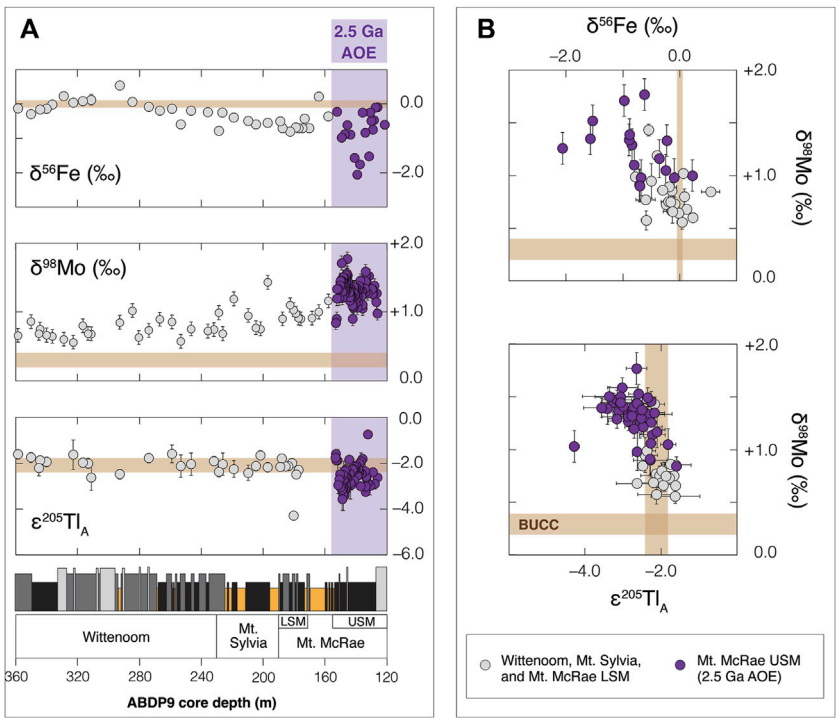

FIGURE 8 | (A) Updated Fe, Mo, and Tl isotope compilation from ABDP9 shales and **(B)** cross-plots of these same data. Brown rectangles in each panel signify bulk upper continental crust values for each isotope system (crustal δ^{98}Mo value comes from Willbold and Elliott 2017; all other crustal value references can be found in the text). Iron isotope data are from Ostrander et al. (2022) and this study. Molybdenum isotope data are from Duan et al. (2010) and Ostrander et al. (2019; 2020). Thallium isotope data are from Ostrander et al. (2019) and this study. AOE = Archean Oxidation Event, BUCC = bulk upper continental crust, LSM = lower shale member, and USM = upper shale member.

plausible Fe oxide formation pathways during the late-Archean (photo-oxidation (Cairns-Smith 1978; Braterman et al., 1983) and photo-ferrotrophy (Widdel et al., 1993; Konhauser et al., 2002)), and no Fe redox change is required during hydrothermal Fe delivery and pyrite formation.

U Isotope Data

Barring coincidence, near-crustal bulk-shale δ^{238}U values require limited isotopic fractionation of U during the late-Archean, at least in this paleo-setting and potentially beyond it. This concept is further supported by the persistently low U abundances in the Wittenoom and Mt. Sylvia formations, which imply a limited availability of dissolved U in the contemporaneous ocean. A good linear correlation is found between bulk-shale U and Al abundances (R^2 = 0.73; **Figure 7A**) that strongly suggests, like the Al, the U in these shales is of detrital origin. For some added context, the correlation between bulk-shale Fe and Al abundances is significantly weaker (R^2 < 0.01), indicating relatively minor

detrital Fe contributions (as already concluded above for most samples). As discussed in the introduction, minimal sedimentary U accumulation and U isotopic fractionation are predictable consequences of a low-O_2 late-Archean Earth (Kendall et al., 2013; Brüske et al., 2020).

Tl Isotope Data

Measured $\varepsilon^{205}Tl_A$ values are very likely representative of overlying seawater at the time of deposition. First, it is unlikely that these $\varepsilon^{205}Tl_A$ are diluted by detrital material. The dilute nitric acid partial digestion that is used to isolate Tl in shale samples from authigenic phases (namely, pyrite; Nielsen et al., 2011) is unlikely to liberate significant amounts of Tl from detrital phases. In support of this notion, we find no correlation whatsoever between $\varepsilon^{205}Tl_A$ values and Al abundances ($R^2 << 0.01$). Furthermore, invariant $\varepsilon^{205}Tl_A$ values are found in shales from both the Wittenoom and Mt. Sylvia formations despite authigenic Tl concentrations that span an order of magnitude (ranging from 0.1 to 1.2 μg/g; **Figure 4**). This wide concentration range suggests that a Tl-rich and most likely non-detrital phase was present in the shales. This Tl-rich phase was most likely pyrite—a notion that gains strong support from the correlation revealed between authigenic Tl abundances and shale pyrite Fe contents ($R^2 = 0.84$; **Figure 7B**). Second, sediments from the three anoxic settings studied thus far using Tl isotopes (Black Sea, Cariaco Basin, and Santa Barbara Basin) always capture the overlying seawater $\varepsilon^{205}Tl$ value (Owens et al., 2017; Fan et al., 2020; Chen et al., 2022). It is reasonable to assume that, by analogy, our shales deposited under comparable conditions also captured the overlying seawater $\varepsilon^{205}Tl$ value. Because the ancient depositional basin is thought to have maintained a strong connection with the open ocean (Morris and Horowitz 1983), this seawater $\varepsilon^{205}Tl$ value was at least a regional signature, and potentially global.

The most straightforward interpretation of a near-crustal seawater $\varepsilon^{205}Tl$ signature is limited Mn oxide burial over large areas of the late-Archean seafloor. In a widely anoxic ocean with limited Mn oxide burial, it would be extremely difficult to drive a change in the seawater $\varepsilon^{205}Tl$ value away from that of global oceanic inputs (discussed in the introduction). Global oceanic inputs today have an average estimated $\varepsilon^{205}Tl$ value ($\varepsilon^{205}Tl_{IN} = -1.8$; Nielsen et al., 2017) indistinguishable from the bulk upper continental crust ($\varepsilon^{205}Tl_{BUCC} = -2.1 \pm 0.3$; Nielsen et al., 2005)—and also indistinguishable from the shale $\varepsilon^{205}Tl_A$ values in the Wittenoom and Mt. Sylvia formations ($\varepsilon^{205}Tl_A = -2.0 \pm 0.6$). In order to prevent Mn oxide burial, O_2 penetration into sediment porewaters must have been minimal to non-existent over at least regions of the ancient seafloor.

Common Themes

To recap, the main findings from each isotopic dataset are:

1) There are multiple possible interpretations of the $\delta^{56}Fe$ data, but none that require strictly aerobic processes.
2) The $\delta^{238}U$ data require limited mobilization and isotopic fractionation of U, and therefore minimal U(IV) oxidation in surface environments.
3) The $\varepsilon^{205}Tl_A$ data require limited Mn oxide burial over at least regions of the seafloor, and by extension minimal O_2 penetration into marine sediment porewaters.

As a collective, the three separate isotope datasets point strongly toward a low-O_2 Earth surface between ~2.6 and ~2.5 Ga. Our sampling resolution is coarse, averaging one shale sample about every 7 m in ABDP9, and therefore an average of one shale sample about every five million-years of late-Archean time (assuming constant sedimentation rates and an age of our samples between 2.6 and 2.5 Ga). Our data therefore speak most directly to the long-term "background" redox state of Earth's oceans and atmosphere, over the many tens-of-millions of years leading up to 2.5 Ga. Given the coarse sampling resolution, our data do not preclude short-term changes in atmospheric or ocean redox, for example, those that might have occurred over hundreds-of-thousands to single-millions of years (e.g., AOEs; Ostrander et al., 2021).

Information about the background atmospheric redox state can be gleaned most directly from the U data. Multiple previous studies have leveraged the geochemical distribution of U and U-bearing minerals in the sedimentary record to reconstruct past pO_2 (e.g., Sverjensky and Lee, 2010; Johnson et al., 2014). According to the modeling results of Sverjensky and Lee, (2010), oxidation and mobilization of U from the predominant U-bearing crustal mineral, uraninite, requires more strongly oxidizing conditions compared to that required for the oxidation and mobilization of other metals hosted in sulfide minerals, such as Mo and Re. In support of this notion, evidence of mild seawater Mo accumulation and isotopic fractionation is also found in the Wittenoom and Mt. Sylvia formations in ABDP9 (Ostrander et al., 2020), and evidence of mild seawater Re accumulation is found in the coeval equivalent Nauga Formation from South Africa (Kendall et al., 2010). Yet, corresponding evidence of appreciable seawater U accumulation is not found in the Wittenoom and Mt. Sylvia formations (this study), nor is it found in the Nauga Formation (Kendall et al., 2015a; Brüske et al., 2020).

The results of a recent Mo mass-balance and weathering model suggest a pO_2 lower-limit of $10^{-6.3}$ PAL is required to explain the Neoarchean sedimentary Mo record (Johnson et al., 2021). Paired together with available MIF-S pO_2 upper limits across the same timeframe (10^{-6} PAL; Catling and Zahnle, 2020), this could suggest a narrow window of pO_2 between $10^{-6.3}$ PAL and 10^{-6} PAL is required to explain our U data, a window permitted also by pO_2 quantifications derived from the presence of rounded uraninite grains in late-Archean sandstones ($pO_2 < 10^{-3.8}$ PAL; Johnson et al., 2014). Alternatively, and perhaps more likely, atmospheric O_2 accumulation during deposition of the Wittenoom and Mt. Sylvia formations was spatially heterogenous, occurring only near the sites of O_2 production (within and near oases and benthic mats; Olson et al., 2013; Lalonde and Konhauser 2015; Sumner et al., 2015; Liu et al., 2019; Johnson et al., 2021).

Information about the background marine redox state can be gleaned from the Fe and Tl data. As discussed earlier, many scenarios requiring the formation of Fe oxide minerals elsewhere

in the ocean can explain the lower δ^{56}Fe values in the Mt. Sylvia Formation (as low as −0.78 ± 0.08‰). Trends to comparable (Eroglu et al., 2018) and even lower δ^{56}Fe values (as low as −1.47‰; Czaja et al., 2012) are found in roughly contemporaneous strata from South Africa and interpreted in a similar manner. The ubiquitous nature of banded-iron formations (BIFs) in the Neoarchean sedimentary record provides even more convincing evidence of extensive Fe oxide formation in late-Archean sediments (summarized in Konhauser et al., 2017). Yet, the Tl isotope data do not support widespread Mn oxide formation or burial in marine sediments between 2.6 and 2.5 Ga, nor are any Mn oxide BIF equivalents found in the Neoarchean record (Johnson et al., 2016). Formation and burial of Fe oxides in marine sediments occurs under less oxidizing conditions than does formation and burial of Mn oxides (Froelich et al., 1979), with a prerequisite for the latter probably being strong O_2 penetration into marine sediments (Calvert and Pederson, 1996). It therefore seems that regional, if not global marine sediments were sufficiently oxidizing between ~2.6 and ~2.5 Ga to promote long-term Fe oxide burial, but insufficiently oxidizing to promote long-term Mn oxide burial.

Interestingly, strong shale Re enrichments are found together with low-to-negligible Mo enrichments in the 2.6–2.5 Ga Nauga Formation (Kendall et al., 2010). Today, this geochemical pattern is found in marine sediments where O_2 penetration depths are relatively shallow (<~1 cm; Morford et al., 2005) and when Fe oxides are the primary electron acceptor (Morford et al., 2012), under slightly more reducing conditions than those permissive of Mn oxide formation (Froelich et al., 1979). Sedimentary environments like those identified by Kendall et al. (2010) could therefore have been commonplace during the late-Archean, proximal to sites of O_2 accumulation along ocean margins, without requiring any substantial Mn oxide burial (and thus no substantial Tl isotope fractionation effect). Further work should test this hypothesis.

It may be that only during pronounced AOEs—like that captured in the upper shale member of the overlying Mt. McRae Shale at 2.5 Ga—did Mn oxide burial become a widespread phenomenon in Archean marine sediments. This hypothesis gains support from an updated compilation of Fe, Mo, and Tl isotope data for ABDP9 shales (**Figure 8**). With minor exception, bulk-shale δ^{56}Fe and δ^{98}Mo values are lower and higher, respectively, than their crustal equivalents throughout the ABDP9 core (**Figure 8A**). It is already established that the formation of Fe oxide minerals in late-Archean oceans likely played some role in driving the light δ^{56}Fe values. Iron oxide formation can also explain the heavy δ^{98}Mo values because a strong negative isotope fractionation effect is imparted on Mo during sorption to Fe oxides (average $\Delta^{98}Mo_{oxide\text{-}solution}$ = −0.8‰ to −2.2‰; Goldberg et al., 2009). In sum, Fe oxide formation would have led to the preferential removal of heavier-mass Fe isotopes and lighter-mass Mo isotopes from seawater, driving anti-correlated seawater δ^{56}Fe and δ^{98}Mo trends that could then be transferred to sediments (apparent across all ABDP9 shale units in the upper panel of **Figure 8B**). In contrast, evidence attributable strictly to Mn oxide burial—consistently light $\varepsilon^{205}Tl_A$ values—is found only in the upper shale member of the Mt. McRae Shale, coincident with the 2.5 Ga AOE (**Figure 8A**). Especially heavy δ^{98}Mo values in the upper shale member (see the lower panel in **Figure 8B**) also support Mn oxide burial because these minerals impart an especially strong negative Mo isotope fractionation effect ($\Delta^{98}Mo_{oxide\text{-}solution}$ = −2.4‰ to −2.9‰; Wasylenki et al., 2008).

The persistently low background O_2 levels implied by our dataset are not only followed by an AOE, but also preceded by one (~2.65 Ga; Koehler et al., 2018). When viewed in this broader context, our data support the idea that Earth's initial oxygenation was no singular event, but instead a protracted process that unfolded in fits-and-starts over many hundreds-of-millions of years (summarized in Lyons et al., 2014; Ostrander et al., 2021).

CONCLUSION

The early history of O_2 on Earth is slowly coming into focus. Here, by applying three complementary heavy metal isotope systems to a rare continuous shale sequence deposited between ~2.6 and 2.5 Ga, we were able to place O_2 constraints on the eve of Earth's GOE. Negligible U accumulation and isotopic fractionation imply limited oxidative weathering of uraninite, and therefore either homogenous and low pO_2 between about $10^{-6.3}$ and 10^{-6} PAL or heterogeneous and spatially restricted O_2 accumulation nearest the sites of O_2 production. Slightly variable bulk-shale δ^{56}Fe (and δ^{98}Mo) values in the same samples, together with invariant $\varepsilon^{205}Tl_A$, imply widespread marine redox conditions sufficiently oxidizing for sedimentary Fe oxide burial (not strictly aerobic, and with weak O_2 penetration when aerobic), but insufficient for sedimentary Mn oxide burial (aerobic, with strong O_2 penetration). Given the temporal context of our shales, and our sampling resolution, these redox constraints are pertinent over ten-million-year timescales between about 2.6 and 2.5 Ga.

The low background O_2 levels implied by our dataset do not seem to be representative of the Archean as a whole. Compelling evidence has been presented for the production and mild accumulation of O_2 at Earth's surface at various times during the Archean. The most notable and pertinent examples are the many lines of independent evidence supporting transient AOEs slightly before (~2.65 Ga) and immediately after (~2.50 Ga) the timeframe studied here (summarized in Ostrander et al., 2021). As a collective, this emerging evidence points strongly toward a dynamic and protracted initial oxygenation of the Earth system.

DATA AVAILABILITY STATEMENT

The original contributions presented in the study are included in the article/**Supplementary Material**, further inquiries can be directed to the corresponding author.

AUTHOR CONTRIBUTIONS

CO, BK, GG, SN and AA developed the project idea. CO processed samples and performed Fe, Tl and U isotope analyses with contributions from WZ. CO wrote the manuscript with contributions from BK and SN.

FUNDING

This work was supported financially by the NSF Frontiers in Earth System Dynamics program award NSF EAR-1338810 (AA), a Woods Hole Oceanographic Institution Postdoctoral Scholarship (CO), a NSERC Discovery Grant (RGPIN-435930) and the Canada Research Chair program (BK), and a NASA Exobiology award 80NSSC20K0615 (SN).

SUPPLEMENTARY MATERIAL

The Supplementary Material for this article can be found online at: https://www.frontiersin.org/articles/10.3389/feart.2022.833609/full#supplementary-material

REFERENCES

Anbar, A. D., Duan, Y., Lyons, T. W., Arnold, G. L., Kendall, B., Creaser, R. A., et al. (2007). A Whiff of Oxygen before the Great Oxidation Event? *Science* 317, 1903–1906. doi:10.1126/science.1140325

Arnold, G. L., Weyer, S., and Anbar, A. D. (2004). Fe Isotope Variations in Natural Materials Measured Using High Mass Resolution Multiple Collector ICPMS. *Anal. Chem.* 76, 322–327. doi:10.1021/ac034601v

Asael, D., Tissot, F. L. H., Reinhard, C. T., Rouxel, O., Dauphas, N., Lyons, T. W., et al. (2013). Coupled Molybdenum, Iron and Uranium Stable Isotopes as Oceanic Paleoredox Proxies during the Paleoproterozoic Shunga Event. *Chem. Geology.* 362, 193–210. doi:10.1016/j.chemgeo.2013.08.003

Baker, R. G. A., Rehkämper, M., Hinkley, T. K., Nielsen, S. G., and Toutain, J. P. (2009). Investigation of Thallium Fluxes from Subaerial Volcanism-Implications for the Present and Past Mass Balance of Thallium in the Oceans. *Geochimica et Cosmochimica Acta* 73, 6340–6359. doi:10.1016/j.gca.2009.07.014

Beard, B. L., Johnson, C. M., Skulan, J. L., Nealson, K. H., Cox, L., and Sun, H. (2003). Application of Fe Isotopes to Tracing the Geochemical and Biological Cycling of Fe. *Chem. Geology.* 195, 87–117. doi:10.1016/s0009-2541(02)00390-x

Braterman, P. S., Cairns-Smith, A. G., and Sloper, R. W. (1983). Photo-oxidation of Hydrated Fe2+-Significance for Banded Iron Formations. *Nature* 303, 163–164. doi:10.1038/303163a0

Brocks, J. J., Buick, R., Logan, G. A., and Summons, R. E. (2003). Composition and Syngeneity of Molecular Fossils from the 2.78 to 2.45 Billion-Year-Old Mount Bruce Supergroup, Pilbara Craton, Western Australia. *Geochimica et Cosmochimica Acta* 67, 4289–4319. doi:10.1016/s0016-7037(03)00208-4

Brüske, A., Martin, A. N., Rammensee, P., Eroglu, S., Lazarov, M., Albut, G., et al. (2020). The Onset of Oxidative Weathering Traced by Uranium Isotopes. *Precambrian Res.* 338, 105583. doi:10.1016/j.precamres.2019.105583

Busigny, V., Planavsky, N. J., Jézéquel, D., Crowe, S., Louvat, P., Moureau, J., et al. (2014). Iron Isotopes in an Archean Ocean Analogue. *Geochimica et Cosmochimica Acta* 133, 443–462. doi:10.1016/j.gca.2014.03.004

Cairns-Smith, A. G. (1978). Precambrian Solution Photochemistry, Inverse Segregation, and Banded Iron Formations. *Nature* 276, 807–808. doi:10.1038/276807a0

Calvert, S. E., and Pedersen, T. F. (1996). Sedimentary Geochemistry of Manganese; Implications for the Environment of Formation of Manganiferous Black Shales. *Econ. Geology.* 91, 36–47. doi:10.2113/gsecongeo.91.1.36

Catling, D. C., and Zahnle, K. J. (2020). The Archean Atmosphere. *Sci. Adv.* 6, eaax1420. doi:10.1126/sciadv.aax1420

Chen, X., Li, S., Newby, S. M., Lyons, T. W., Wu, F., and Owens, J. D. (2022). Iron and Manganese Shuttle Has No Effect on Sedimentary Thallium and Vanadium Isotope Signatures in Black Sea Sediments. *Geochimica et Cosmochimica Acta* 317, 218–233. doi:10.1016/j.gca.2021.11.010

Chen, X., Tissot, F. L. H., Jansen, M. F., Bekker, A., Liu, C. X., Nie, N. X., et al. (2021). The Uranium Isotopic Record of Shales and Carbonates through Geologic Time. *Geochimica et Cosmochimica Acta* 300, 164–191. doi:10.1016/j.gca.2021.01.040

Craddock, P. R., and Dauphas, N. (2011). Iron Isotopic Compositions of Geological Reference Materials and Chondrites. *Geostandards Geoanalytical Res.* 35, 101–123. doi:10.1111/j.1751-908x.2010.00085.x

Czaja, A. D., Johnson, C. M., Roden, E. E., Beard, B. L., Voegelin, A. R., Nägler, T. F., et al. (2012). Evidence for Free Oxygen in the Neoarchean Ocean Based on Coupled Iron-Molybdenum Isotope Fractionation. *Geochimica et Cosmochimica Acta* 86, 118–137. doi:10.1016/j.gca.2012.03.007

Dauphas, N., John, S. G., and Rouxel, O. (2017). Iron Isotope Systematics. *Rev. Mineralogy Geochem.* 82, 415–510. doi:10.2138/rmg.2017.82.11

Duan, Y., Anbar, A. D., Arnold, G. L., Lyons, T. W., Gordon, G. W., and Kendall, B. (2010). Molybdenum Isotope Evidence for Mild Environmental Oxygenation before the Great Oxidation Event. *Geochimica et Cosmochimica Acta* 74, 6655–6668. doi:10.1016/j.gca.2010.08.035

Eigenbrode, J. L., and Freeman, K. H. (2006). Late Archean Rise of Aerobic Microbial Ecosystems. *Proc. Natl. Acad. Sci. U.S.A.* 103, 15759–15764. doi:10.1073/pnas.0607540103

Eroglu, S., Schoenberg, R., Pascarelli, S., Beukes, N. J., Kleinhanns, I. C., and Swanner, E. D. (2018). Open Ocean vs. Continentally-Derived Iron Cycles along the Neoarchean Campbellrand-Malmani Carbonate Platform, South Africa. *Am. J. Sci.* 318, 367–408. doi:10.2475/04.2018.01

Eroglu, S., Schoenberg, R., Wille, M., Beukes, N., and Taubald, H. (2015). Geochemical Stratigraphy, Sedimentology, and Mo Isotope Systematics of the Ca. 2.58-2.50 Ga-old Transvaal Supergroup Carbonate Platform, South Africa. *Precambrian Res.* 266, 27–46. doi:10.1016/j.precamres.2015.04.014

Eroglu, S., van Zuilen, M. A., Taubald, H., Drost, K., Wille, M., Swanner, E. D., et al. (2017). Depth-dependent δ13C Trends in Platform and Slope Settings of the Campbellrand-Malmani Carbonate Platform and Possible Implications for Early Earth Oxygenation. *Precambrian Res.* 302, 122–139. doi:10.1016/j.precamres.2017.09.018

Fan, H., Nielsen, S. G., Owens, J. D., Auro, M., Shu, Y., Hardisty, D. S., et al. (2020). Constraining Oceanic Oxygenation during the Shuram Excursion in South China Using Thallium Isotopes. *Geobiology* 18, 348–365. doi:10.1111/gbi.12379

Fischer, W. W., Schroeder, S., Lacassie, J. P., Beukes, N. J., Goldberg, T., Strauss, H., et al. (2009). Isotopic Constraints on the Late Archean Carbon Cycle from the Transvaal Supergroup along the Western Margin of the Kaapvaal Craton, South Africa. *Precambrian Res.* 169, 15–27. doi:10.1016/j.precamres.2008.10.010

Froelich, P. N., Klinkhammer, G. P., Bender, M. L., Luedtke, N. A., Heath, G. R., Cullen, D., et al. (1979). Early Oxidation of Organic Matter in Pelagic Sediments of the Eastern Equatorial Atlantic: Suboxic Diagenesis. *Geochimica et Cosmochimica Acta* 43, 1075–1090. doi:10.1016/0016-7037(79)90095-4

Garvin, J., Buick, R., Anbar, A. D., Arnold, G. L., and Kaufman, A. J. (2009). Isotopic Evidence for an Aerobic Nitrogen Cycle in the Latest Archean. *Science* 323, 1045–1048. doi:10.1126/science.1165675

Godfrey, L. V., and Falkowski, P. G. (2009). The Cycling and Redox State of Nitrogen in the Archaean Ocean. *Nat. Geosci* 2, 725–729. doi:10.1038/ngeo633

Goldberg, T., Archer, C., Vance, D., and Poulton, S. W. (2009). Mo Isotope Fractionation during Adsorption to Fe (Oxyhydr)oxides. *Geochimica et Cosmochimica Acta* 73, 6502–6516. doi:10.1016/j.gca.2009.08.004

Gregory, D. D., Large, R. R., Halpin, J. A., Steadman, J. A., Hickman, A. H., Ireland, T. R., et al. (2015). The Chemical Conditions of the Late Archean Hamersley basin Inferred from Whole Rock and Pyrite Geochemistry with Δ33S and δ34S Isotope Analyses. *Geochimica et Cosmochimica Acta* 149, 223–250. doi:10.1016/j.gca.2014.10.023

Guilbaud, R., Butler, I. B., and Ellam, R. M. (2011). Abiotic Pyrite Formation Produces a Large Fe Isotope Fractionation. *Science* 332, 1548–1551. doi:10.1126/science.1202924

Heard, A. W., Dauphas, N., Guilbaud, R., Rouxel, O. J., Butler, I. B., Nie, N. X., et al. (2020). Triple Iron Isotope Constraints on the Role of Ocean Iron Sinks in Early Atmospheric Oxygenation. *Science* 370, 446–449. doi:10.1126/science.aaz8821

Johnson, A. C., Ostrander, C. M., Romaniello, S. J., Reinhard, C. T., Greaney, A. T., Lyons, T. W., et al. (2021). Reconciling Evidence of Oxidative Weathering and Atmospheric Anoxia on Archean Earth. *Sci. Adv.* 7, eabj0108. doi:10.1126/sciadv.abj0108

Johnson, C. M., Beard, B. L., and Roden, E. E. (2008). The Iron Isotope Fingerprints of Redox and Biogeochemical Cycling in Modern and Ancient Earth. *Annu. Rev. Earth Planet. Sci.* 36, 457–493. doi:10.1146/annurev.earth.36.031207.124139

Johnson, J. E., Gerpheide, A., Lamb, M. P., and Fischer, W. W. (2014). O2constraints from Paleoproterozoic Detrital Pyrite and Uraninite. *Geol. Soc. America Bull.* 126, 813–830. doi:10.1130/b30949.1

Johnson, J. E., Webb, S. M., Ma, C., and Fischer, W. W. (2016). Manganese Mineralogy and Diagenesis in the Sedimentary Rock Record. *Geochimica et Cosmochimica Acta* 173, 210–231. doi:10.1016/j.gca.2015.10.027

Kaufman, A. J., Johnston, D. T., Farquhar, J., Masterson, A. L., Lyons, T. W., Bates, S., et al. (2007). Late Archean Biospheric Oxygenation and Atmospheric Evolution. *Science* 317, 1900–1903. doi:10.1126/science.1138700

Kendall, B., Creaser, R. A., Reinhard, C. T., Lyons, T. W., and Anbar, A. D. (2015a). Transient Episodes of Mild Environmental Oxygenation and Oxidative continental Weathering during the Late Archean. *Sci. Adv.* 1, e1500777. doi:10.1126/sciadv.1500777

Kendall, B., Brennecka, G. A., Weyer, S., and Anbar, A. D. (2013). Uranium Isotope Fractionation Suggests Oxidative Uranium Mobilization at 2.50 Ga. *Chem. Geology.* 362, 105–114. doi:10.1016/j.chemgeo.2013.08.010

Kendall, B., Dahl, T. W., and Anbar, A. D. (2017). The Stable Isotope Geochemistry of Molybdenum. *Rev. Mineralogy Geochem.* 82, 683–732. doi:10.2138/rmg.2017.82.16

Kendall, B., Komiya, T., Lyons, T. W., Bates, S. M., Gordon, G. W., Romaniello, S. J., et al. (2015b). Uranium and Molybdenum Isotope Evidence for an Episode of Widespread Ocean Oxygenation during the Late Ediacaran Period. *Geochimica et Cosmochimica Acta* 156, 173–193. doi:10.1016/j.gca.2015.02.025

Kendall, B., Reinhard, C. T., Lyons, T. W., Kaufman, A. J., Poulton, S. W., and Anbar, A. D. (2010). Pervasive Oxygenation along Late Archaean Ocean Margins. *Nat. Geosci* 3, 647–652. doi:10.1038/ngeo942

Koehler, M. C., Buick, R., Kipp, M. A., Stüeken, E. E., and Zaloumis, J. (2018). Transient Surface Ocean Oxygenation Recorded in the ~2.66-Ga Jeerinah Formation, Australia. *Proc. Natl. Acad. Sci. U.S.A.* 115, 7711–7716. doi:10.1073/pnas.1720820115

Konhauser, K. O., Hamade, T., Raiswell, R., Morris, R. C., Grant Ferris, F., Southam, G., et al. (2002). Could Bacteria Have Formed the Precambrian Banded Iron Formations? *Geol* 30, 1079–1082. doi:10.1130/0091-7613(2002)030<1079:cbhftp>2.0.co;2

Konhauser, K. O., Planavsky, N. J., Hardisty, D. S., Robbins, L. J., Warchola, T. J., Haugaard, R., et al. (2017). Iron Formations: A Global Record of Neoarchaean to Palaeoproterozoic Environmental History. *Earth-Science Rev.* 172, 140–177. doi:10.1016/j.earscirev.2017.06.012

Kopp, R. E., Kirschvink, J. L., Hilburn, I. A., and Nash, C. Z. (2005). The Paleoproterozoic Snowball Earth: a Climate Disaster Triggered by the Evolution of Oxygenic Photosynthesis. *Proc. Natl. Acad. Sci. U.S.A.* 102, 11131–11136. doi:10.1073/pnas.0504878102

Ku, T.-L., Mathieu, G. G., and Knauss, K. G. (1977). Uranium in Open Ocean: Concentration and Isotopic Composition. *Deep Sea Res.* 24, 1005–1017. doi:10.1016/0146-6291(77)90571-9

Kurzweil, F., Wille, M., Schoenberg, R., Taubald, H., and Van Kranendonk, M. J. (2015). Continuously Increasing δ 98 Mo Values in Neoarchean Black Shales and Iron Formations from the Hamersley Basin. *Geochimica et Cosmochimica Acta* 164, 523–542. doi:10.1016/j.gca.2015.05.009

Lalonde, S. V., and Konhauser, K. O. (2015). Benthic Perspective on Earth's Oldest Evidence for Oxygenic Photosynthesis. *Proc. Natl. Acad. Sci. U.S.A.* 112, 995–1000. doi:10.1073/pnas.1415718112

Langmuir, D. (1978). Uranium Solution-mineral Equilibria at Low Temperatures with Applications to Sedimentary Ore Deposits. *Geochimica et Cosmochimica Acta* 42, 547–569. doi:10.1016/0016-7037(78)90001-7

Liu, P., Harman, C. E., Kasting, J. F., Hu, Y., and Wang, J. (2019). Can Organic Haze and O2 Plumes Explain Patterns of Sulfur Mass-independent Fractionation during the Archean? *Earth Planet. Sci. Lett.* 526, 115767. doi:10.1016/j.epsl.2019.115767

Lough, A. J. M., Klar, J. K., Homoky, W. B., Comer-Warner, S. A., Milton, J. A., Connelly, D. P., et al. (2017). Opposing Authigenic Controls on the Isotopic Signature of Dissolved Iron in Hydrothermal Plumes. *Geochimica et Cosmochimica Acta* 202, 1–20. doi:10.1016/j.gca.2016.12.022

Lyons, T. W., Reinhard, C. T., and Planavsky, N. J. (2014). The Rise of Oxygen in Earth's Early Ocean and Atmosphere. *Nature* 506, 307–315. doi:10.1038/nature13068

Lyons, T. W., and Severmann, S. (2006). A Critical Look at Iron Paleoredox Proxies: New Insights from Modern Euxinic marine Basins. *Geochimica et Cosmochimica Acta* 70, 5698–5722. doi:10.1016/j.gca.2006.08.021

Meixnerová, J., Blum, J. D., Johnson, M. W., Stüeken, E. E., Kipp, M. A., Anbar, A. D., et al. (2021). Mercury Abundance and Isotopic Composition Indicate Subaerial Volcanism Prior to the End-Archean "Whiff" of Oxygen. *Proc. Natl. Acad. Sci.* 118, e2107511118. doi:10.1073/pnas.2107511118

Morford, J. L., Emerson, S. R., Breckel, E. J., and Kim, S. H. (2005). Diagenesis of Oxyanions (V, U, Re, and Mo) in Pore Waters and Sediments from a continental Margin. *Geochimica et Cosmochimica Acta* 69, 5021–5032. doi:10.1016/j.gca.2005.05.015

Morford, J. L., Martin, W. R., and Carney, C. M. (2012). Rhenium Geochemical Cycling: Insights from continental Margins. *Chem. Geology.* 324-325, 73–86. doi:10.1016/j.chemgeo.2011.12.014

Morris, R. C., and Horwitz, R. C. (1983). The Origin of the Iron-Formation-Rich Hamersley Group of Western Australia - Deposition on a Platform. *Precambrian Res.* 21, 273–297. doi:10.1016/0301-9268(83)90044-x

Nielsen, S. G., Goff, M., Hesselbo, S. P., Jenkyns, H. C., LaRowe, D. E., and Lee, C.-T. A. (2011). Thallium Isotopes in Early Diagenetic Pyrite - A Paleoredox Proxy? *Geochimica et Cosmochimica Acta* 75, 6690–6704. doi:10.1016/j.gca.2011.07.047

Nielsen, S. G., Rehkämper, M., Baker, J., and Halliday, A. N. (2004). The Precise and Accurate Determination of Thallium Isotope Compositions and Concentrations for Water Samples by MC-ICPMS. *Chem. Geology.* 204, 109–124. doi:10.1016/j.chemgeo.2003.11.006

Nielsen, S. G., Rehkämper, M., Norman, M. D., Halliday, A. N., and Harrison, D. (2006b). Thallium Isotopic Evidence for Ferromanganese Sediments in the Mantle Source of Hawaiian Basalts. *Nature* 439, 314–317. doi:10.1038/nature04450

Nielsen, S. G., Rehkämper, M., Porcelli, D., Andersson, P., Halliday, A. N., Swarzenski, P. W., et al. (2005). Thallium Isotope Composition of the Upper continental Crust and Rivers-An Investigation of the continental Sources of Dissolved marine Thallium. *Geochimica et Cosmochimica Acta* 69, 2007–2019. doi:10.1016/j.gca.2004.10.025

Nielsen, S. G., Rehkämper, M., and Prytulak, J. (2017). Investigation and Application of Thallium Isotope Fractionation. *Rev. Mineralogy Geochem.* 82, 759–798. doi:10.2138/rmg.2017.82.18

Nielsen, S. G., Rehkämper, M., Teagle, D. A. H., Butterfield, D. A., Alt, J. C., and Halliday, A. N. (2006a). Hydrothermal Fluid Fluxes Calculated from the Isotopic Mass Balance of Thallium in the Ocean Crust. *Earth Planet. Sci. Lett.* 251, 120–133. doi:10.1016/j.epsl.2006.09.002

Nielsen, S. G., Wasylenki, L. E., Rehkämper, M., Peacock, C. L., Xue, Z., and Moon, E. M. (2013). Towards an Understanding of Thallium Isotope Fractionation during Adsorption to Manganese Oxides. *Geochimica et Cosmochimica Acta* 117, 252–265. doi:10.1016/j.gca.2013.05.004

Ohmoto, H., Watanabe, Y., Ikemi, H., Poulson, S. R., and Taylor, B. E. (2006). Sulphur Isotope Evidence for an Oxic Archaean Atmosphere. *Nature* 442, 908–911. doi:10.1038/nature05044

Olson, S. L., Kump, L. R., and Kasting, J. F. (2013). Quantifying the Areal Extent and Dissolved Oxygen Concentrations of Archean Oxygen Oases. *Chem. Geology.* 362, 35–43. doi:10.1016/j.chemgeo.2013.08.012

Olson, S. L., Ostrander, C. M., Gregory, D. D., Roy, M., Anbar, A. D., and Lyons, T. W. (2019). Volcanically Modulated Pyrite Burial and Ocean-Atmosphere Oxidation. *Earth Planet. Sci. Lett.* 506, 417–427. doi:10.1016/j.epsl.2018.11.015

Ostrander, C. M., Owens, J. D., and Nielsen, S. G. (2017). Constraining the Rate of Oceanic Deoxygenation Leading up to a Cretaceous Oceanic Anoxic Event (OAE-2: ~94 Ma). *Sci. Adv.* 3, e1701020. doi:10.1126/sciadv.1701020

Ostrander, C. M., Johnson, A. C., and Anbar, A. D. (2021). Earth's First Redox Revolution. *Annu. Rev. Earth Planet. Sci.* 49, 337–366. doi:10.1146/annurev-earth-072020-055249

Ostrander, C. M., Kendall, B., Olson, S. L., Lyons, T. W., Gordon, G. W., Romaniello, S. J., et al. (2020). An Expanded Shale δ98Mo Record Permits Recurrent Shallow marine Oxygenation during the Neoarchean. *Chem. Geology*. 532, 119391. doi:10.1016/j.chemgeo.2019.119391

Ostrander, C. M., Nielsen, S. G., Owens, J. D., Kendall, B., Gordon, G. W., Romaniello, S. J., et al. (2019). Fully Oxygenated Water Columns over continental Shelves before the Great Oxidation Event. *Nat. Geosci.* 12, 186–191. doi:10.1038/s41561-019-0309-7

Ostrander, C. M., Severmann, S., Gordon, G. W., Kendall, B., Lyons, T. W., Zheng, W., et al. (2022). Significance of 56Fe Depletions in Late-Archean Shales and Pyrite. *Geochimica et Cosmochimica Acta* 316, 87–104. doi:10.1016/j.gca.2021.10.013

Owens, J. D., Nielsen, S. G., Horner, T. J., Ostrander, C. M., and Peterson, L. C. (2017). Thallium-isotopic Compositions of Euxinic Sediments as a Proxy for Global Manganese-Oxide Burial. *Geochimica et Cosmochimica Acta* 213, 291–307. doi:10.1016/j.gca.2017.06.041

Partin, C. A., Bekker, A., Planavsky, N. J., Scott, C. T., Gill, B. C., Li, C., et al. (2013). Large-scale Fluctuations in Precambrian Atmospheric and Oceanic Oxygen Levels from the Record of U in Shales. *Earth Planet. Sci. Lett.* 369-370, 284–293. doi:10.1016/j.epsl.2013.03.031

Peacock, C. L., and Moon, E. M. (2012). Oxidative Scavenging of Thallium by Birnessite: Explanation for Thallium Enrichment and Stable Isotope Fractionation in marine Ferromanganese Precipitates. *Geochimica et Cosmochimica Acta* 84, 297–313. doi:10.1016/j.gca.2012.01.036

Raiswell, R., Hardisty, D. S., Lyons, T. W., Canfield, D. E., Owens, J. D., Planavsky, N. J., et al. (2018). The Iron Paleoredox Proxies: A Guide to the Pitfalls, Problems and Proper Practice. *Am. J. Sci.* 318, 491–526. doi:10.2475/05.2018.03

Rehkämper, M., Frank, M., Hein, J. R., Porcelli, D., Halliday, A., Ingri, J., et al. (2002). Thallium Isotope Variations in Seawater and Hydrogenetic, Diagenetic, and Hydrothermal Ferromanganese Deposits. *Earth Planet. Sci. Lett.* 197, 65–81. doi:10.1016/S0012-821X(02)00462-4

Rehkämper, M., and Halliday, A. N. (1999). The Precise Measurement of Tl Isotopic Compositions by MC-ICPMS: Applications to the Analysis of Geological Materials and Meteorites. *Geochimica et Cosmochimica Acta* 63, 935–944. doi:10.1016/S0016-7037(98)00312-3

Reinhard, C. T., Raiswell, R., Scott, C., Anbar, A. D., and Lyons, T. W. (2009). A Late Archean Sulfidic Sea Stimulated by Early Oxidative Weathering of the Continents. *Science* 326, 713–716. doi:10.1126/science.1176711

Rouxel, O. J., Bekker, A., and Edwards, K. J. (2005). Iron Isotope Constraints on the Archean and Paleoproterozoic Ocean Redox State. *Science* 307, 1088–1091. doi:10.1126/science.1105692

Rudnick, R. L., and Gao, S. (2003). "Composition of the continental Crust,".in *The Crust*. Editor R. L. Rudnick (Elsevier), 3, 1–64. doi:10.1016/b0-08-043751-6/03016-4

Sarmiento, J. L., and Gruber, N. (2006). *Ocean Biogeochemical Dynamics*. Princeton, NJ, USA: Princeton University Press.

Scholz, F., Severmann, S., McManus, J., and Hensen, C. (2014). Beyond the Black Sea Paradigm: The Sedimentary Fingerprint of an Open-marine Iron Shuttle. *Geochimica et Cosmochimica Acta* 127, 368–380. doi:10.1016/j.gca.2013.11.041

Severmann, S., Lyons, T. W., Anbar, A., McManus, J., and Gordon, G. (2008). Modern Iron Isotope Perspective on the Benthic Iron Shuttle and the Redox Evolution of Ancient Oceans. *Geol* 36, 487–490. doi:10.1130/g24670a.1

Stüeken, E. E., Buick, R., and Anbar, A. D. (2015). Selenium Isotopes Support Free O_2 in the Latest Archean. *Geology* 43, 259–262. doi:10.1130/G36218.1

Stüeken, E. E., Catling, D. C., and Buick, R. (2012). Contributions to Late Archaean sulphur Cycling by Life on Land. *Nat. Geosci.* 5, 722–725. doi:10.1038/ngeo1585

Sumner, D. Y., Hawes, I., Mackey, T. J., Jungblut, A. D., and Doran, P. T. (2015). Antarctic Microbial Mats: a Modern Analog for Archean Lacustrine Oxygen Oases. *Geology* 43, 887–890. doi:10.1130/g36966.1

Sverjensky, D. A., and Lee, N. (2010). The Great Oxidation Event and mineral Diversification. *Elements* 6, 31–36. doi:10.2113/gselements.6.1.31

Tissot, F. L. H., and Dauphas, N. (2015). Uranium Isotopic Compositions of the Crust and Ocean: Age Corrections, U Budget and Global Extent of Modern Anoxia. *Geochimica et Cosmochimica Acta* 167, 113–143. doi:10.1016/j.gca.2015.06.034

Trendall, A. F., Compston, W., Nelson, D. R., De Laeter, J. R., and Bennett, V. C. (2004). SHRIMP Zircon Ages Constraining the Depositional Chronology of the Hamersley Group, Western Australia*. *Aust. J. Earth Sci.* 51, 621–644. doi:10.1111/j.1400-0952.2004.01082.x

Trendall, A. F., Nelson, D. R., De Laeter, J. R., and Hassler, S. W. (1998). Precise Zircon U-Pb Ages from the Marra Mamba Iron Formation and Wittenoom Formation, Hamersley Group, Western Australia. *Aust. J. Earth Sci.* 45, 137–142. doi:10.1080/08120099808728374

Wang, X., Ossa Ossa, F., Hofmann, A., Agangi, A., Paprika, D., and Planavsky, N. J. (2020). Uranium Isotope Evidence for Mesoarchean Biological Oxygen Production in Shallow marine and continental Settings. *Earth Planet. Sci. Lett.* 551, 116583. doi:10.1016/j.epsl.2020.116583

Wang, X., Planavsky, N. J., Hofmann, A., Saupe, E. E., De Corte, B. P., Philippot, P., et al. (2018). A Mesoarchean Shift in Uranium Isotope Systematics. *Geochimica et Cosmochimica Acta* 238, 438–452. doi:10.1016/j.gca.2018.07.024

Wasylenki, L. E., Rolfe, B. A., Weeks, C. L., Spiro, T. G., and Anbar, A. D. (2008). Experimental Investigation of the Effects of Temperature and Ionic Strength on Mo Isotope Fractionation during Adsorption to Manganese Oxides. *Geochimica et Cosmochimica Acta* 72, 5997–6005. doi:10.1016/j.gca.2008.08.027

Welch, S. A., Beard, B. L., Johnson, C. M., and Braterman, P. S. (2003). Kinetic and Equilibrium Fe Isotope Fractionation between Aqueous Fe(II) and Fe(III). *Geochimica et Cosmochimica Acta* 67, 4231–4250. doi:10.1016/s0016-7037(03)00266-7

Weyer, S., Anbar, A. D., Gerdes, A., Gordon, G. W., Algeo, T. J., and Boyle, E. A. (2008). Natural Fractionation of 238U/235U. *Geochimica et Cosmochimica Acta* 72, 345–359. doi:10.1016/j.gca.2007.11.012

Widdel, F., Schnell, S., Heising, S., Ehrenreich, A., Assmus, B., and Schink, B. (1993). Ferrous Iron Oxidation by Anoxygenic Phototrophic Bacteria. *Nature* 362, 834–836. doi:10.1038/362834a0

Willbold, M., and Elliott, T. (2017). Molybdenum Isotope Variations in Magmatic Rocks. *Chem. Geology*. 449, 253–268. doi:10.1016/j.chemgeo.2016.12.011

Wille, M., Kramers, J. D., Nägler, T. F., Beukes, N. J., Schröder, S., Meisel, T., et al. (2007). Evidence for a Gradual Rise of Oxygen between 2.6 and 2.5Ga from Mo Isotopes and Re-PGE Signatures in Shales. *Geochimica et Cosmochimica Acta* 71, 2417–2435. doi:10.1016/j.gca.2007.02.019

Woodhead, J. D., Hergt, J. M., and Simonson, B. M. (1998). Isotopic Dating of an Archean Bolide Impact Horizon, Hamersley Basin, Western Australia. *Geol* 26, 47–50. doi:10.1130/0091-7613(1998)026<0047:idoaab>2.3.co;2

Zhang, F., Xiao, S., Kendall, B., Romaniello, S. J., Cui, H., Meyer, M., et al. (2018). Extensive marine Anoxia during the Terminal Ediacaran Period. *Sci. Adv.* 4, eaan8983. doi:10.1126/sciadv.aan8983

Conflict of Interest: The authors declare that the research was conducted in the absence of any commercial or financial relationships that could be construed as a potential conflict of interest.

Publisher's Note: All claims expressed in this article are solely those of the authors and do not necessarily represent those of their affiliated organizations, or those of the publisher, the editors, and the reviewers. Any product that may be evaluated in this article, or any claim that may be made by its manufacturer, is not guaranteed or endorsed by the publisher.